

## MSEC2009-84046

### NUMERICAL SIMULATIONS AND ANALYSIS OF THE THERMAL EFFECTS ON SILICON CARBIDE DURING DUCTILE MODE MICRO-LASER ASSISTED MACHINING

**Saurabh R. Virkar<sup>#</sup>**

Industrial and Manufacturing Engineering  
Western Michigan University  
Kalamazoo, MI-49008, USA.

**John A. Patten<sup>\*</sup>**

Manufacturing Engineering  
Western Michigan University  
Kalamazoo, MI-49008, USA.

#### ABSTRACT

Various 2-D numerical simulations were carried out using the commercial software AdvantEdge Versions 5.2 and 5.3 to model ductile mode micro-Laser Assisted Machining ( $\mu$ -LAM) of Silicon Carbide (4H-SiC). The cutting tool is a single point diamond. The workpiece material (SiC) is heated locally by a laser beam, which passes through the diamond tool tip. The workpiece is heated beyond the thermal softening point in order to study the effect of increased temperature. The cutting and thrust forces are reduced when machining is done above the thermal softening temperature. The simulations were carried out for two cases at different temperatures above and below the thermal softening point to study the effect of  $\mu$ -LAM on the cutting and thrust forces. In the first case both the tool and workpiece material were heated to study the behavior at elevated temperatures. In the second case, a thermal boundary condition was provided on the top surface of the workpiece to simulate the laser heating effect keeping the tool at room temperature (20° C). In both cases the chip formation was observed and the changes in cutting and thrust forces were evaluated. The simulation results indicate a significant decrease in machining forces if Silicon Carbide is heated beyond the thermal softening temperature thus demonstrating the benefits of  $\mu$ -LAM process.

Keywords: Precision machining, Single Point Diamond Turning, Thermal softening, 4H Silicon Carbide

#### 1 INTRODUCTION

Silicon Carbide (SiC) is an advanced engineered ceramic and an alternative to semiconducting Silicon (Si) for operation at elevated temperatures and high power applications. Some of SiC's beneficial properties include: chemical resistance, high temperature resistance, extreme hardness and high stiffness [1]. Also Silicon carbide is one of the non oxide ceramics that are found in various commercial applications and hence it has a good corrosion and erosion resistance [2]. SiC has a relatively high hardness, ~ 26 GPa and is nominally a brittle material [13]. Hence machining of SiC is difficult as the cutting forces may be very high, which can damage the tool as well as impart

<sup>#</sup> [saurabh.r.virkar@wmich.edu](mailto:saurabh.r.virkar@wmich.edu)

<sup>\*</sup> [john.patten@wmich.edu](mailto:john.patten@wmich.edu)

damage (fracture) into the workpiece. The classic property and benefit of SiC is that it retains its strength even at elevated temperatures, which imposes additional challenges for laser assisted (elevated temperature) machining. Current limitations for brittle material machining include the high cost of processing and product reliability. The cost is mainly due to the high tool cost, rapid tool wear, long machining time, low production rate and the manufacturing of satisfactory surface figure and form. The low product reliability is primarily due to the occurrence of surface/subsurface damage and brittle fracture.

Laser Assisted Machining (LAM) is a promising way of lowering the material strength during machining [5]. LAM can also increase the material removal rates while maintaining the workpiece surface quality. In LAM processes, the workpiece is heated locally by a laser, past its thermal softening point, and then ductile mode machining is done on the thermally softened surface [5]. In  $\mu$ -LAM, the laser beam passes through the diamond tool, thus heating the surface just below the tool tip in the chip formation zone [20]. The heating effect produced is at the microscopic scale and hence the laser power required to heat the workpiece is less than in macro LAM processes [8]. During LAM processing the workpiece is deformed below the fracture strength, thereby enabling a visco-plastic flow rather than brittle fracture [5]. The workpiece used in this study is crystalline 4H-SiC. This simulation work was done to obtain the behavior of single crystal SiC at elevated temperatures to perform ductile mode machining. The objective of this study is to simulate the change in the chip formation and study the resultant machining forces with and without laser heating. The workpiece is heated above the thermal softening point to analyze the change in cutting and thrust forces during machining. The cutting pressure also decreases as the workpiece temperature increases by the laser heating effect. As these ceramic materials are expensive, simulations prove to be a suitable tool to complement the physical experiments. The simulations also provide sufficient data to relate to the experiment results.

## 2 MATHEMATICAL MODEL

### 2.1 Introduction

As the workpiece is heated locally there is thermal softening and subsequent ductile material removal during machining. There is also a High Pressure Phase Transformation (HPPT) at the tool-chip interface, and the resultant phase obtained is ductile (metallic or amorphous) in certain ceramics such as Silicon Nitride and SiC [4]. The ductile material removal below the thermal softening point is due to HPPT. The existence of high pressure phase beyond the thermal softening point is not yet reported. By confining the scope of the simulation to the ductile mode of material removal, it is possible to use the metal machining simulation software AdvantEdge to predict the behavior of SiC. The software currently only includes ductile or plastic deformation and does not consider a fracture criterion or brittle material removal mechanisms. In the ductile mode (even for ceramics), the software can be used to accurately predict the forces and pressures generated by the tool-workpiece interaction, for a given set of process conditions assuming an appropriate material model is used [7].

Material properties are specified in the model which includes elastic and plastic behavior, heat transfer, thermal softening as well as strain rate sensitivity. The simulation (material model) uses the Drucker-Prager model to accommodate the pressure induced phase transformation and the resultant plastic/ductile behavior [7].

#### 2.1.1 Elastic Plastic Behavior

The elastic behavior is specified by providing the Elastic (Young's) modulus and Poisson's ratio. The strain hardening behavior for the Drucker-Prager model is defined as

$$g(\varepsilon^p) = \sigma_0 \Theta(T) \left(1 + \frac{\varepsilon^p}{\varepsilon_0^p}\right)^{1/n} \quad (1)$$

where  $\sigma_0$  is the initial yield stress,  $\varepsilon^p$  is the plastic strain,  $\varepsilon_0^p$  is the reference plastic strain,  $\Theta(T)$  is the thermal softening function and  $n$  is the strain hardening exponent. The initial yield stress is calculated using the Drucker-Prager yield criterion [7].

#### 2.1.2 Thermal Softening Behavior

The thermal softening function  $\Theta(T)$  is defined as

$$\Theta(T) = c_0 + c_1 T + c_2 T^2 + c_3 T^3 + c_4 T^4 + c_5 T^5 \quad \text{if } T < T_{cut} \quad (2)$$

$$\Theta(T) = \Theta(T_{cut}) \left(1 - \frac{T - T_{cut}}{T_{melt} - T_{cut}}\right) \quad \text{if } T \geq T_{cut} \quad (3)$$

The polynomial coefficients  $c_0$  through  $c_5$  are fit to a 5<sup>th</sup> order polynomial,  $T$  is the temperature,  $T_{cut}$  is the linear cutoff temperature and  $T_{melt}$  is the melting temperature.

For the polynomial shown in equation (2),  $c_0$  is set to 1 while  $c_1$  through  $c_5$  are set to zero in the AdvantEdge software. Thus the value of thermal softening is 1 for temperatures below or equal to the cutoff temperature of the material, reaching a value of zero at the melting temperature as seen in figure 1. This simple model is a current

limitation of the simulation software and was used to study the thermal effects on SiC above the thermal softening temperature.

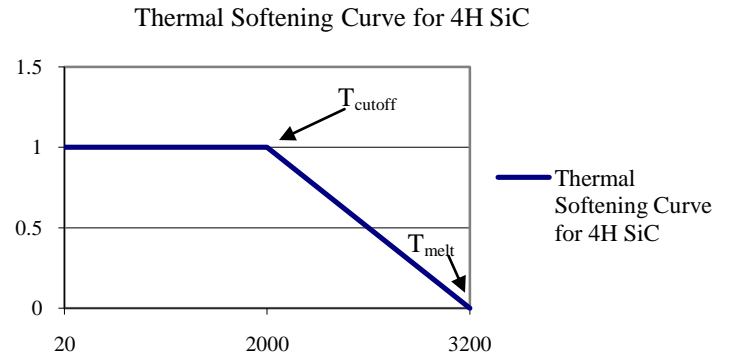


Figure 1 Thermal Softening Curve for 4H-SiC

Note: The temperature values  $T_{cutoff}$  and  $T_{melt}$  are estimated based on different values from various references [8-16]

#### 2.1.3 Strain Rate Sensitivity

The strain rate sensitivity is given by

$$\left(1 + \frac{\dot{\varepsilon}^p}{\dot{\varepsilon}_0^p}\right) = \left[\frac{\bar{\sigma}}{g(\varepsilon^p)}\right]^{m_1}, \quad \text{if } \dot{\varepsilon}^p \leq \dot{\varepsilon}_t^p \quad (4)$$

$$\left(1 + \frac{\dot{\varepsilon}^p}{\dot{\varepsilon}_0^p}\right) \left[1 + \frac{\dot{\varepsilon}_t^p}{\dot{\varepsilon}_0^p}\right]^{\frac{m_2}{m_1}} = \left[\frac{\bar{\sigma}}{g(\varepsilon^p)}\right]^{m_2}, \quad \text{if } \dot{\varepsilon}^p > \dot{\varepsilon}_t^p \quad (5)$$

where  $\bar{\sigma}$  is the effective von Mises stress,  $g$  is the flow stress,  $\dot{\varepsilon}^p$  is the accumulated plastic strain rate,  $\dot{\varepsilon}_0^p$  is the reference plastic strain rate, and  $m_1$  and  $m_2$  are low and high strain rate sensitivity exponents, respectively.  $\dot{\varepsilon}_t^p$  is the threshold strain rate which separates the two regimes. The pertinent workpiece material properties are given in Table 1.

The strain rate sensitivity (refer to Figure 2) is normalized to the initial yield stress [7].

Table 1 Workpiece material properties (Ref. [8])

Material properties	Value	Units
Elastic Modulus, E	330	GPa
Poisson's ratio	0.212	-
Hardness, H	26	GPa
Initial yield stress, $\sigma_0$	16.25	GPa
Reference plastic strain, $\varepsilon_0^p$	$\sigma_0/E$	-
Accumulated plastic strain, $\varepsilon^p$	1	-
Strain hardening exponent, n	50	-
Low strain rate sensitivity exponent, $m_1$	100	-
High strain rate sensitivity exponent, $m_2$	100	-
Threshold strain rate, $\dot{\varepsilon}_t^p$	1E7	sec <sup>-1</sup>

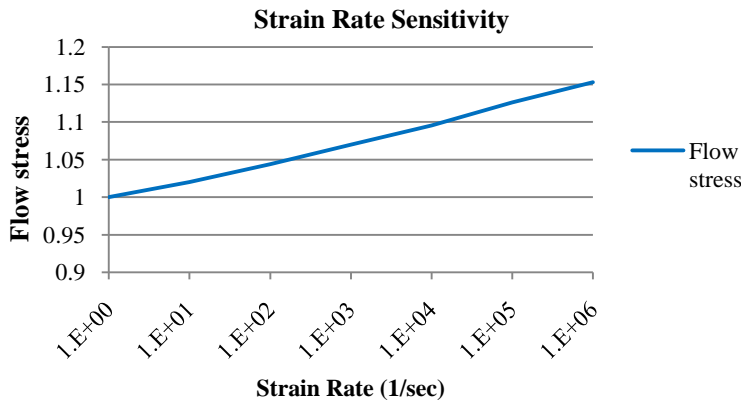


Figure 2 Strain rate sensitivity normalized to initial yield stress

## 2.2 Determination of Initial Yield Stress

To determine the initial yield stress, a pressure sensitive Drucker-Prager model as proposed by Ajarapu et al. (2004) was specified as detailed below.

The Drucker-Prager yield criterion is given by

$$\sqrt{3J_2} + I_1\alpha - \kappa = 0 \quad (5)$$

$J_2$  is the second invariant of the deviatoric stress tensor, given by

$$J_2 = \frac{1}{6}[(\sigma_1 - \sigma_2)^2 + (\sigma_2 - \sigma_3)^2 + (\sigma_3 - \sigma_1)^2] \quad (6)$$

$I_1$  ( $I_1 = \sigma_1 + \sigma_2 + \sigma_3$ ) is the first invariant of stress tensor,  $\alpha$  is the pressure sensitivity coefficient,  $\kappa$  is the initial yield stress. The quantity  $\kappa$  is given by

$$\kappa = \frac{2\sigma_t\sigma_c}{\sigma_t + \sigma_c} \quad (7)$$

where  $\sigma_t$  and  $\sigma_c$  are the yield strength in tension and compression, respectively. The quantity  $\kappa$  is equal to the flow stress in the case when  $\sigma_c = \sigma_t$ , i.e. no pressure dependency.

The hardness of SiC material is taken as 26 GPa [9, 15] and the tensile yield stress is calculated to be 11.82 GPa based on a proposed value of  $H/2.2$  [18]. The compressive yield ( $\sigma_c$ ) is set to equal the hardness of the material [8].

For a uniaxial stress state ( $\sigma_2$  and  $\sigma_3$  are zero),

$$I_1 = \sigma_1 \quad (8)$$

From equation (8) we get,

$$J_2 = \frac{\sigma_1^2}{3} \quad (9)$$

From equation (9),  $\kappa$  equals 16.25 GPa and from equation (5),  $\alpha$  equals 0.375. These two parameters are set in the software material model to provide a pressure sensitive (Drucker-Prager) yield criterion.

## 3. SIMULATION MODEL

The simulation method is based upon a 2-D Lagrangian finite-element machining model assuming plane strain conditions [19]. The simulations were carried out by specifying the material properties for polycrystalline  $\alpha$ -4H-SiC. Thus, the constitutive model does not

incorporate crystallographic planes/orientations and treats the material as elastic-plastic and ductile. To reflect the ductile behavior in ceramics, promoted by the HPPT, a pressure sensitive Drucker-Prager constitutive model as explained in section 2.2 is used.

The objective of these simulations was to study ductile machining behavior of single crystal SiC above its thermal softening temperature. For this study, the crystalline dependency of the brittle behavior of SiC is not included in the model, as the primary goal is to study the thermal softening and resultant plastic and ductile material response. The simulations were carried out in two stages. In the first stage both the tool and workpiece were heated and, in the second stage a thermal boundary condition was provided on the top surface of the workpiece to simulate the laser heating effect. (Note: The simulation software does not provide for the direct incorporation of the laser heat source, thus the heating effect is modeled with these thermal conditions) The simulation input consists of the workpiece and tool dimensions and their mechanical and thermal properties as described in the next section. The tool and workpiece material models used in this simulation work are similar to comparison study between numerical simulations and single point diamond turning experiments done by Patten et al. (2008), which demonstrates that the material models are quite reliable [10,20].

## 3.1 Workpiece model and Properties

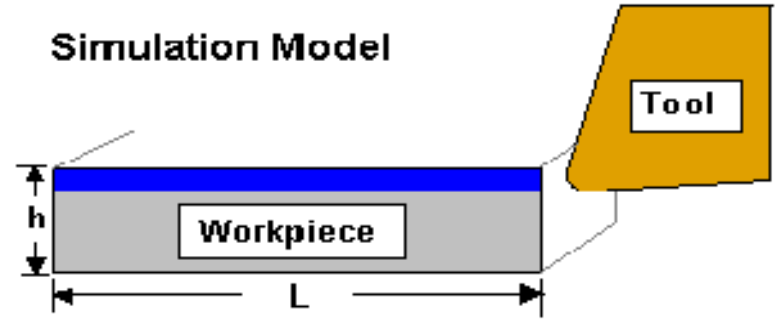


Figure 3 Simulation Model

The workpiece was made long enough ( $L = 0.08$  mm) to ensure that the length of cut ( $loc$ ) would allow steady state conditions to be achieved. The height ( $h = 0.02$  mm) of the workpiece was much larger (between 10 to 100 times) in comparison to the feed ( $f$ ) or uncut chip thickness ( $t$ ). The boundary conditions of the workpiece surface is assumed to be traction free and constrained in vertical direction. Refer to Figure 3 and 4 for these dimensions.

The thermal properties of the SiC are given in Table 2.

Table 2 Thermal properties of workpiece (SiC) (Ref. [8])

Properties	Value
Thermal Conductivity (W/m ° C)	390
*Thermal Softening temperature (° C)	2000
*Melting temperature (° C)	3200
Initial reference temperature (° C)	20

\* Note: The thermal softening and melting temperature of SiC given in table 2 are estimated based on various references [8-16] to study the behavior of SiC while machining above thermal softening temperature.

## 3.2 Tool Specifications

The tool used is a single point diamond. The tool parameters are given in table 3. The simulations were conducted in 2-D and as a result a round nose tool geometry could not be simulated, therefore the simulated tool cutting edge is flat. The top and rear surfaces of the tool are rigidly fixed with adiabatic conditions. The material model for the

tool is polycrystalline diamond with elastic properties as given in Table 4.

**Table 3 Tool Parameters/Geometry**

Cutting Edge Radius, $r$ , (nm)	100
Rake angle, $\alpha$	-45°
Relief angle, $\beta$	5°
Rake length (mm)	0.0075
Relief length (mm)	0.0075

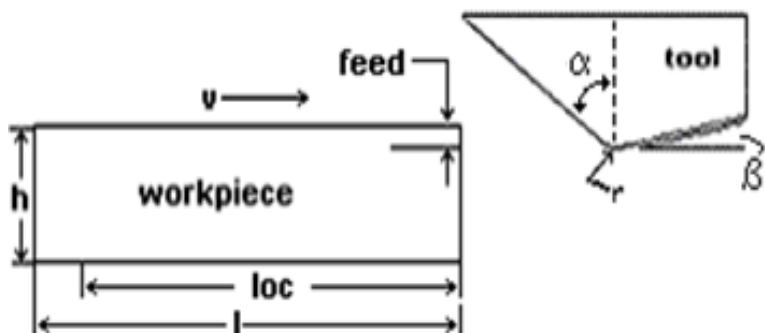


**Figure 4 Tool and Workpiece geometry**

The -45° rake angle creates a high pressure sufficient to accommodate the HPPT, thus the chip formation zone is conducive for ductile deformation [6]. The thermal and mechanical properties of diamond are given in table 4.

**Table 4 Tool Properties (Ref. [8])**

Thermal Conductivity, W/m °C	1500
Heat Capacity, J/kg °C	471.5
Density, kg/m <sup>3</sup>	3520
Elastic Modulus, GPa	1050
Poisson's ratio	0.2

### 3.3 Simulation Process

Process parameters used in the simulations are given in table 5.

**Table 5 Process Parameters**

Parameters	Values
Feed (nm)	500
Coefficient of friction	0.5
Cutting speed (m/s)	1
Depth of cut (mm)	0.02

The simulations were conducted with the values given in Tables 2, 3, 4 and 5. The feed in the 2-D simulation relates to the uncut chip thickness, and the depth of cut refers to the workpiece width. With the given values of high negative rake angle and feed, ductile mode machining was achieved in the experiments performed by Patten et al. (2005). The coefficient of friction was taken as 0.5 however the results are not very sensitive to this value as established in previous research [8]. The simulation results include the cutting and thrust forces that are

used for comparison to evaluate the various machining conditions (primarily the workpiece temperature and the resultant thermal softening effect). All simulated force results are based on achieving steady-state conditions. The initial temperature of the workpiece and tool is set at room temperature (20° C). To study the various effects of heating on SiC, two different conditions were used to study the behavior of SiC. In the first case, both the tool and workpiece were heated. In the second case, a thermal boundary condition was provided on the top surface of workpiece to artificially increase the temperature in an effort to simulate the effect of the  $\mu$ -LAM process. The simulations were carried out at various temperatures above and below the thermal softening point of SiC. The simulation temperatures were 20° C, 1000° C, 1900° C, 2000° C, 2300° C, 2600° C and 3100° C, where 2000° C is the thermal softening temperature as shown in figure 1. The feed and cutting edge radius were kept constant in all simulations. The results of the simulations were viewed in Tecplot [7] which provides temperature, pressure and stress contours along with the cutting and thrust force plots for analysis of the simulation results. At each of the simulated temperatures, the chip formation, force plots and pressure contours are used and compared to evaluate the results.

## 4 RESULTS

In the first case when both the tool and workpiece were heated to the same temperature, the comparisons of the different simulations are made with reference to the simulation at room temperature as shown in figure 5.

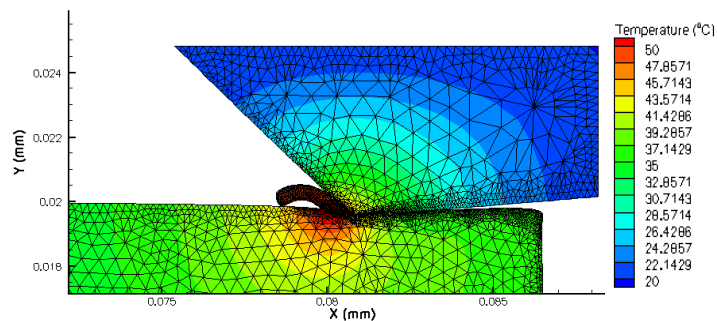


**Figure 5 (At 20° C)**

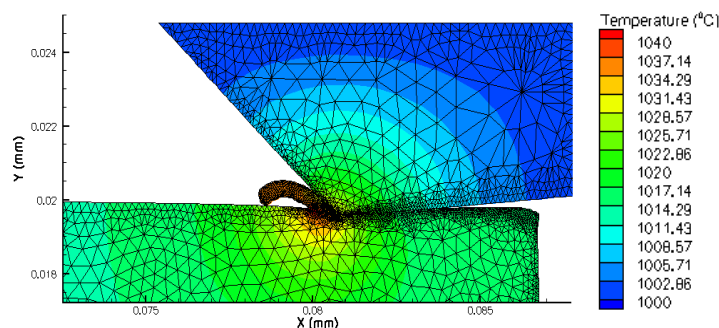


**Figure 6 (At 1000° C)**

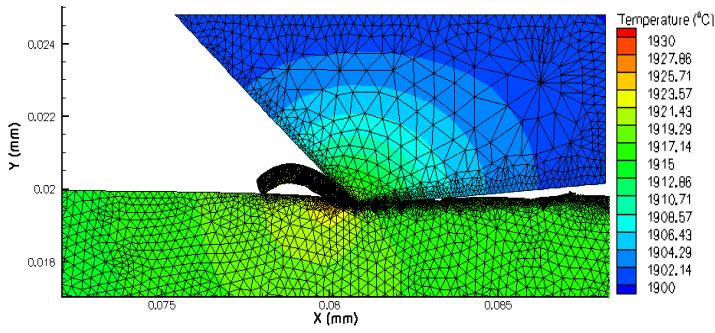


Figure 7 (At 1900° C)

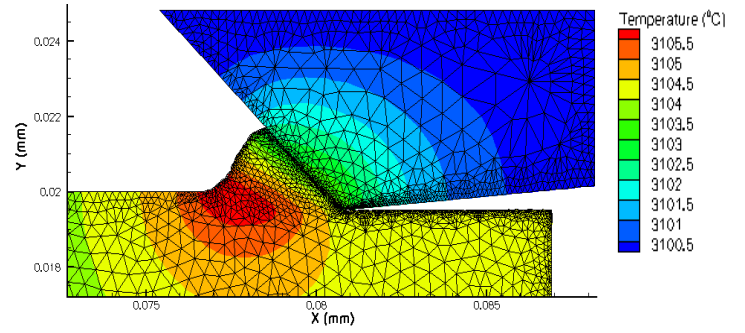


Figure 11 (At 3100° C)

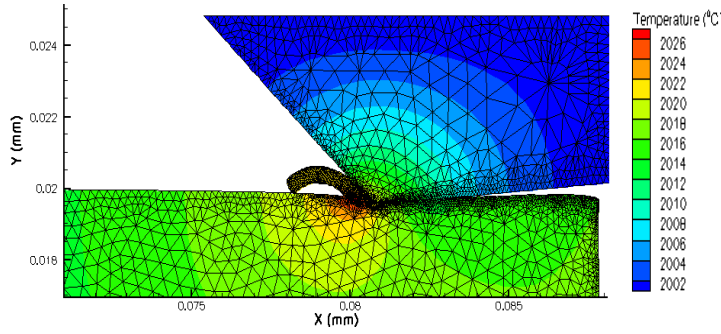


Figure 8 (At 2000° C)

From figures 5-8 it can be seen that from 20 °C until the thermal softening temperature of 2000 °C there is no significant change in the chip formation. Note that the temperature scale changes in each figure, as the minimum temperature is set to the pre-heating temperature. The workpiece undergoes plastic deformation and high pressures are observed at the tool-workpiece interface. Figures 9, 10 and 11 depict the thermal softening behavior as the chip thickness increases due to decrease in the hardness of SiC. The lower cutting forces enhance precision machining through increased ductile material removal. The simulation results are summarized in Table 6

Table 6 Simulation results

Temperature of simulation (°C)	Maximum Cutting Pressure (GPa)	Cutting force (N)	Thrust force (N)
20	27	0.56	0.85
1000	27	0.56	0.84
1900	27	0.53	0.83
2000	27	0.53	0.83
2300	19	0.48	0.67
2600	15	0.41	0.60
3100	2	0.08	0.09

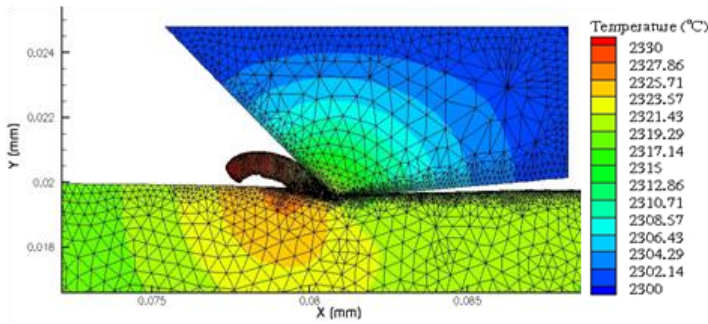


Figure 9 (At 2300° C)

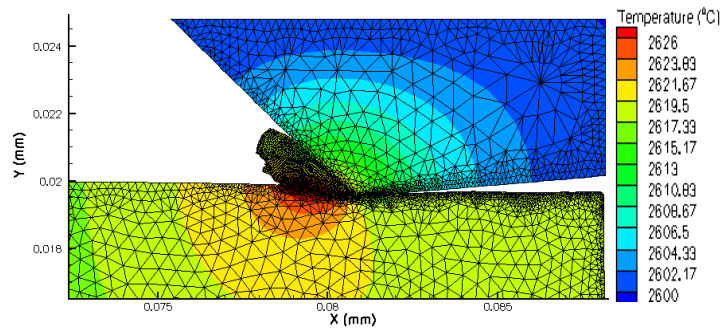


Figure 10 (At 2600° C)

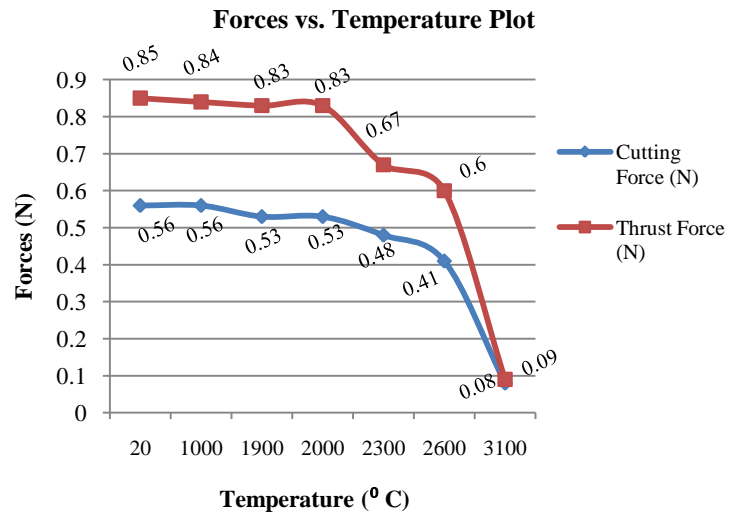


Figure 12

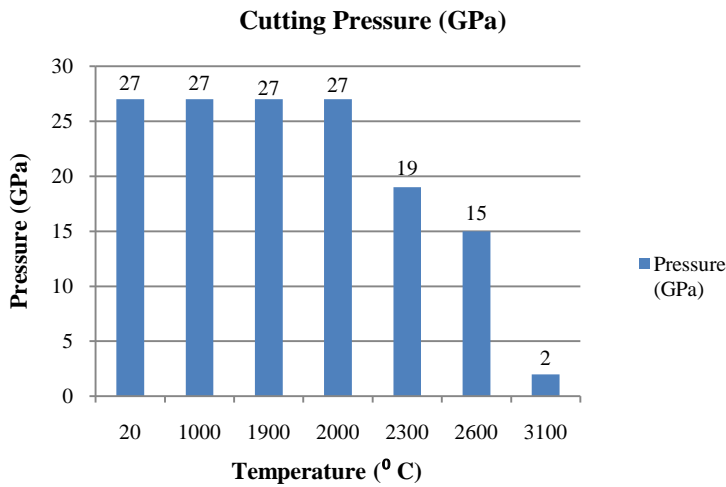


Figure 13

From table 6 and figure 12, it can be seen that there is a sudden change in cutting and thrust forces at temperatures above the thermal softening temperature (2000° C). The change in cutting pressure (refer to Figure 13) is due to a decrease in hardness of SiC above the thermal softening point. To generate a ductile cutting environment through purely applied stress (hydrostatic and shear) required that the pressures at the tool-chip interface be equal to or higher than, the hardness of the material [21], which is taken to be 26 GPa in the material model. In the simulation at 3100 °C the forces and pressure are negligible as the workpiece material is close to the melting temperature (3200 °C). The chip formation is ductile at all temperatures and above the thermal softening temperature, the chip thickness increases.

In the second set of simulations, a thermal boundary condition was provided on the top surface of the workpiece (refer to Figure 14) keeping the tool at room temperature (20° C). These simulations were done to simulate laser assisted machining such that the workpiece is heated by the laser before machining. Note that the temperature scale changes in each figure (Figures 15-20), as the minimum temperature is set at 10° C less than the boundary condition temperature to show the effect of thermal boundary condition on the top surface of the workpiece. The figures 15-20 depict the second stage simulation results.

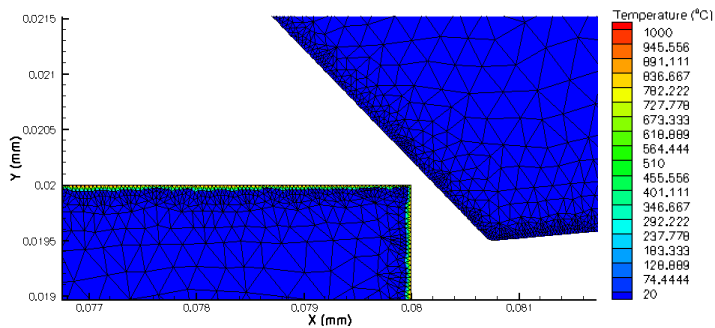


Figure 14 (Workpiece Boundary Condition)

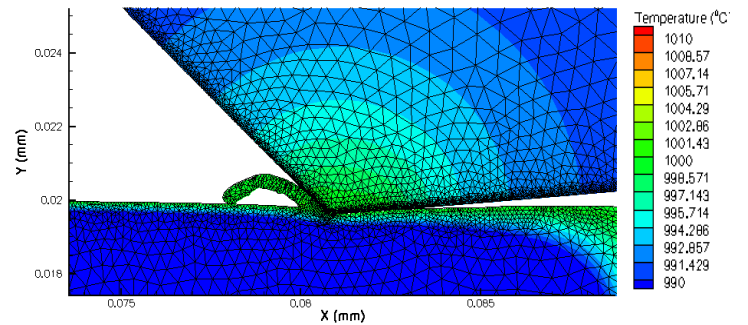


Figure 15 (1000° C boundary condition on workpiece)

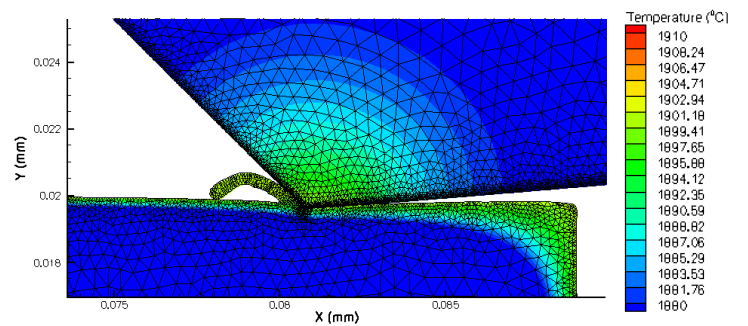


Figure 16 (1900° C boundary condition on workpiece)

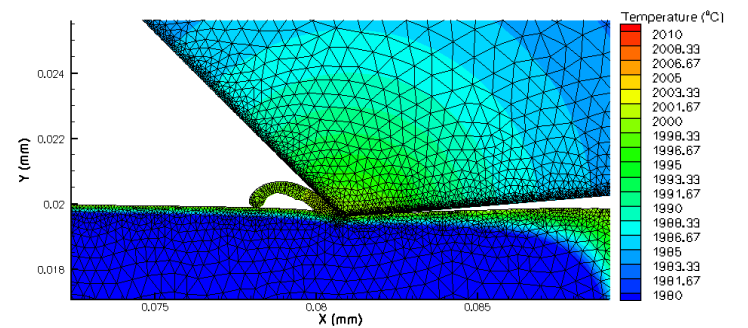


Figure 17 (2000° C boundary condition on workpiece)

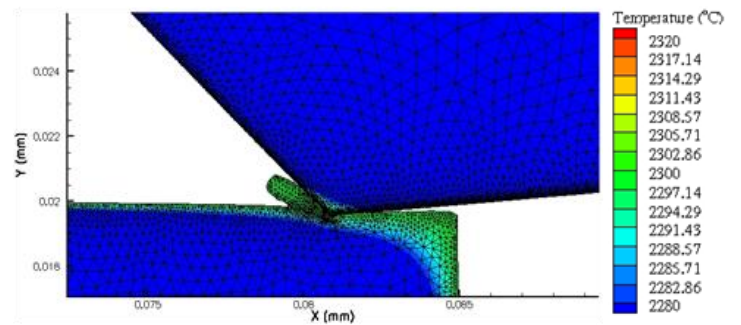


Figure 18 (2300° C boundary condition on workpiece)

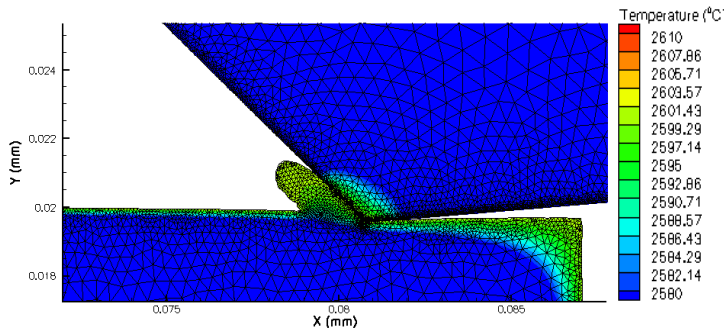


Figure 19 (2600° C boundary condition on workpiece)

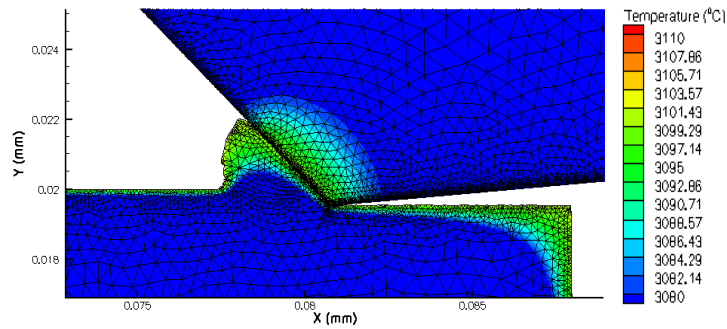


Figure 20 (3100° C boundary condition on workpiece)

In these simulations the thermal boundary condition temperature on the workpiece was varied from 1000° C to 3100° C. In these simulations the tool is also heated (via conduction) approaching the workpiece temperature. As diamond is a good conductor of heat, heat transfer readily takes place from the workpiece to the tool.

Table 7 Results of workpiece boundary condition simulation

Temperature of simulation(°C)	Maximum Cutting Pressure (GPa)	Cutting force (N)	Thrust force (N)
1000	27	0.46	0.78
1900	27	0.45	0.78
2000	26	0.45	0.77
2300	21	0.41	0.61
2600	15	0.33	0.53
3100	4	0.12	0.16

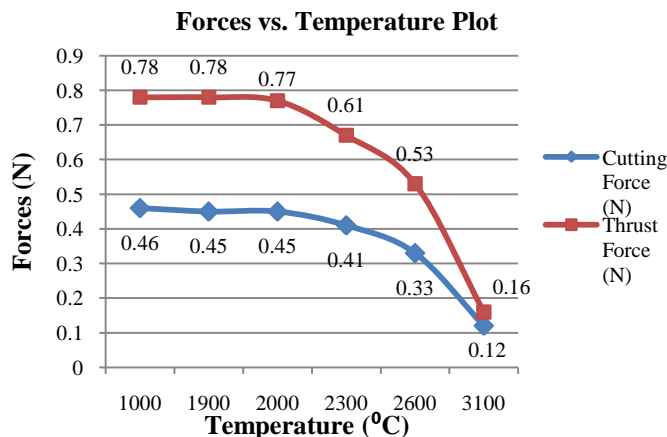


Figure 21

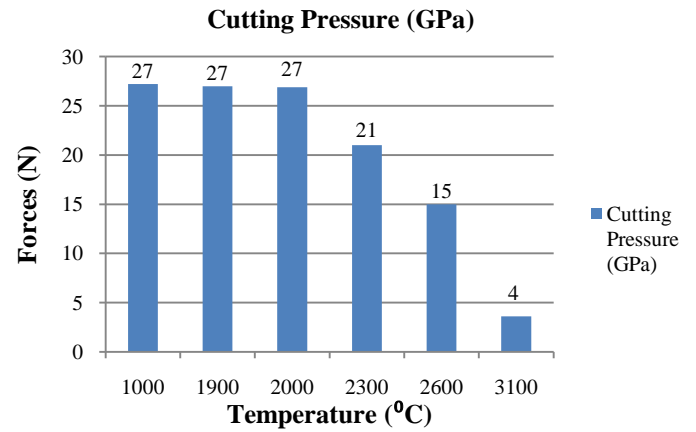


Figure 22 Cutting Pressure Plot

From figure 21, it can be seen that there is a change in cutting and thrust forces above the thermal softening temperature. Theoretically, below the thermal softening temperature (2000° C), the cutting and thrust forces should be approximately remain the same. But in the boundary condition simulations, the cutting and thrust force values also vary slightly due to variation in mesh parameters used in the software. But the behavior of SiC is the same in both cases. The cutting pressure remains high until the thermal softening point (2000° C) as SiC retains its strength and hardness up to the thermal softening point. Above the thermal softening point the strength begins to decrease gradually (as indicated in figure 1) and so do the machining forces. As the temperature approaches the melting temperature (3200° C) the workpiece starts piling up on the rake face of the tool. This phenomena is due to a decrease in hardness and enhanced ductility at elevated temperature [8, 11]

## 5 Conclusions

From the summary of data in tables 6 and 7 it can be seen that there is considerable change in cutting and thrust forces. Tables 8 and 9 indicate the percentage decrease in forces (cutting and thrust respectively) by comparing the simulations at 2600° C to those at 2000° C i.e. above and at the thermal softening temperature.

Table 8

Change in Cutting Forces	Percentage
Both tool and workpiece heated (Case 1)	24%
Boundary condition on workpiece (Case 2)	26%

Table 9

Change in Thrust Forces	Percentage
Both tool and workpiece heated (Case 1)	28%
Boundary condition on workpiece (Case 2)	31%

The drop in cutting and thrust forces when the workpiece is heated above the thermal softening temperature (2000 °C) was significant (24% to 31%) as calculated by considering the values of the cutting and thrust forces at 2000 °C and 2600 °C, as shown in tables 9 and 10.

Below 2000° C the cutting and thrust forces remain almost constant as there is no thermal softening. The chip formation is also seen to change above the thermal softening temperature; above this temperature, the chip formation is quite ductile and hence the chip thickness also increases.

## 6 FUTURE WORK

Current ongoing work includes a thermal boundary condition only on the tool tip. Also 3D scratch test simulations are being conducted to compare with experiments [22]. The scratch tests simulations are being done at various feeds/depths at which the experiments were performed.

## 7 ACKNOWLEDGEMENTS

The authors would like to thank ThirdWave Systems Inc., for their generous support and technical assistance. The authors are also thankful to the National Science Foundation (NSF) for their grant CMMI-0757339.

## 8 REFERENCES

[1] Osiander, R., Champion, J., Darrin, M., 2006, "MEMS and Microstructures in Aerospace Applications," CRC Press, Boca Raton, Florida, US, pp. 321

[2] Srinivasan, M., Ranfaniello, W., 1997, "Acheson Process. Carbide, Nitride and Boride Materials Synthesis and Processing," Weimer, A. W., Ed., Chapman and Hall, London, United Kingdom, pp. 3-42

[3] Patten, J., Cherukuri, H., Yan, J., 2004, "Ductile Regime Machining of Semiconductors and Ceramics", Inst. of Physics Publishing, pp. 616

[4] Patten, J., Bhatt, B., 2006, "Single Point Diamond Turning of CVD coated Silicon Carbide", ASME J. of Manufacturing Science and Engineering, Vol. 127, pp. 522

[5] Shin, Y., C., Pfefferkorn, F., E., Rozzi, J., C., 2000, "Experimental Evaluation of the Laser Assisted Machining of Silicon Nitride Ceramics" ASME, J. of Manufacturing Science, 2000, Vol. 122, pp. 666

[6] Patten, J., A., Gao, W., Yasuto, K., 2005, "Ductile Regime Nanomachining of Single Crystal Silicon Carbide," ASME Journal of Manufacturing Science and Engineering, 127 (8), pp. 522-532

[7] Advantedge User Manual, Version 5.3, 2009

[8] Jacob, J., 2006, "Numerical Simulation on Machining of Silicon Carbide," Master's Thesis, Western Michigan University, MI

[9] Ajjarapu S. K., Cherukuri, H., Patten, J., Brand, C. J., 2004, "Numerical Simulations of Ductile Regime Machining of Silicon Nitride using Drucker Prager model", Proc. Inst. Mech. Engrs., 218 (C), pp. 1-6

[10] Patten, J., Jacob, J., 2008, "Comparison Between Numerical Simulations and Experiments for Single Point Diamond Turning of Single Crystal Silicon Carbide," J. Manufacturing Processes, Vol. 10, pp. 28-33

[11] Shim, S., Jang, J-I., Pharr, G., M., 2008, "Extraction of flow properties of Single Crystal Silicon Carbide by Nanoindentation and Finite Element Simulation," Act. Materia., 58, pp. 3824-3832

[12] Yonenaga, I., 2001, "Thermo-Mechanical Stability of Wide-Bandgap Semiconductors: High Temperature Hardness of SiC, AlN, GaN, ZnO and ZnSe," Physica B. (308-310), pp. 1150-1152

[13] Yonenaga, I., Hoshi, T., Usui, A., 2000, "High Temperature Strength of III-IV Nitride Crystals," J. Phys: Condens. Matter, 14, pp. 12947-12951

[14] Samant, A., V., Zhou, W., L., Pirouz, P., 1998, "Effect of Test Temperature and Strain Rate on the Yield Stress of Monocrystalline 6H-SiC," Phys. Stat. Sol. (a) 166, pp. 155

[15] Tsvetkov, V., F., Allen, S., T., Kong, H., S., Carter, C., H., 1996, "Recent Progress in SiC Crystal Growth," Inst. of Phys. Serial No. 142, pp. 17

[16] CREE material data sheet [www.cree.com](http://www.cree.com)

[17] Naylor, M., G., S., Page, T., F., 1979, "The Effect of Temperature and Load on the Indentation Hardness Behavior of Silicon Carbide Engineering Ceramics," Proc. on Intl. Conf on Erosion of Soil and Impact, pp. 32-1

[18] Gilman, J., J., 1975, "Relationship between Impact Yield Stress and Indentation Hardness," J. of Applied Physics, 46 (4), pp. 1435-1436

[19] Marusich, T., D., Askari, E., 2001, "Modeling Residual Stress and Workpiece Quality in Machined Surfaces," [www.thirdwavesys.com](http://www.thirdwavesys.com)

[20] Patten, J., A., Jacob, J., Bhattacharya, B., Grevstad, A., 2007, "Comparison between numerical simulation and Experiments for Single Point Diamond Turning of Silicon Carbide," Society of Manufacturing Engineers, NAMRC Conf., pp. 2

[21] O'Connor, B., Marsh, E., Couey, J., 2005, "On the Effect of Crystallographic orientations for Ductile Material Removal in Silicon" Precision Engineering, Vol. 29 (1), pp. 124-132

[22] Shayan, A., Poyraz, B., Patten, J., 2009, "Force Analysis, Mechanical Energy and Laser Heating Evaluation of Scratch Tests on Silicon Carbide (4H-SiC) in Micro-Laser Assisted Machining ( $\mu$ -LAM) Process", ASME Manufacturing Science Conference, West Lafayette, Purdue University, submitted